Interacting multiple model state observer-based coordination control of electro-hydraulic composite electronic stability program

Houzhong Zhang and Jiasheng Liang*

Automotive Engineering Research Institute,
Jiangsu University,
Zhenjiang 212013, China
Email: ujs_aeri_motor@163.com
Email: 2211804024@stmail.ujs.edu.cn
*Corresponding author

Haobin Jiang

Automotive Engineering Research Institute,
Jiangsu University,
Zhenjiang 212013, China

and

School of Automobile and Traffic Engineering,
Jiangsu University,
Zhenjiang 212013, China
Email: jianghb@ujs.edu.cn

Xing Xu

Automotive Engineering Research Institute,
Jiangsu University,
Zhenjiang 212013, China
Email: xuxing@mail.ujs.edu.cn

Abstract: In this paper, an electro-hydraulic electronic stability program composite control method is proposed for electric wheeled vehicles based on interacting multiple model state observer. Hydraulic system model, electric-driving wheel model, 2-degrees-of-freedom vehicle reference model and 7-degrees-of-freedom vehicle model are established at the beginning. The necessary state estimations and calculations are also accomplished utilising interacting multiple model unscented Kalman filter. Then, the proposed upper controller calculates the additional yaw moment by fuzzy sliding mode control, and the lower controller distributes the longitudinal force and additional yaw moment based on the quadratic programming optimisation allocation to improve the vehicle handling stability. Finally, using Simulink and CarSim, a joint simulation test platform is established. The simulation results show that the state observer can estimate the driving state parameters accurately enough under various conditions, and coordination control method mentioned in this paper can significantly improve the electric wheeled vehicle's handling stability under extreme conditions.

Keywords: electric wheeled vehicle; electro-hydraulic ESP; composite control method; fuzzy sliding mode control; vehicle handling stability; state observer; interacting multiple model; active safety control; centroid sideslip angle estimation; vehicle state parameter estimation.

Reference to this paper should be made as follows: Zhang, H., Liang, J., Jiang, H. and Xu, X. (2020) 'Interacting multiple model state observer-based coordination control of electro-hydraulic composite electronic stability program', *Int. J. Vehicle Systems Modelling and Testing*, Vol. 14, No. 1, pp.1–25.

Biographical notes: Houzhong Zhang received the PhD in Vehicle Engineering from Tongji University, Shanghai, China, in 2012. He also worked as a Software Engineer in Shanghai Electric Drive Co., Ltd. from 2009 to 2010, responsible for the control and testing of automotive motors. Currently, he is a Master's Supervisor at the Automotive Engineering Research Institute, Jiangsu University. His research interests include distributed drive electric vehicle, simulation and control of vehicle dynamic performance.

Jiasheng Liang received his Bachelor's degree in Engineering College of Anhui Agricultural University, Hefei, Anhui, China, in 2018. Currently, he is pursuing the Master's degree in Automotive Engineering of Jiangsu University. His current research interests include active safety of automobile and state estimation of automobile.

Haobin Jiang received his BS degree in Agricultural Mechanization from Nanjing Agricultural University, Nanjing, China, in 1991, and MS and PhD degrees in Vehicle Engineering from Jiangsu University, Zhenjiang, China, in 1994 and 2000, respectively. His research interests include vehicle dynamic performance analysis and electrical control technology.

Xing Xu received his BS degree in Vehicle Engineering, MS degree in Control Theory and Control Engineering, and PhD in Agricultural Electrification and Automation from Jiangsu University, Zhenjiang, China, in 2002, 2006 and 2010, respectively. Currently, he is currently a Professor and a Doctoral supervisor with the Automotive Engineering Research Institute, Jiangsu University. His research interests include the modelling, identification, optimisation, fault diagnosis, and control of vehicle dynamic systems.

1 Introduction

An electric wheeled vehicle (EWV) is driven by four independently controlled hub motors (Zhu et al., 2012). As the driving force of each wheel is independently controllable and the motors have a fast response and precise control (Jin et al., 2015), research on EWVs has become prominent in automobile factories and universities (Murata, 2010). However, due to limitations associated with motor technology, it is very difficult to control the stability of the vehicle by only using a driving motor at the present stage. On one hand, due to the limited peak torque of the driving motor, a simple coordinated distribution of the motor torque is not sufficient to generate such a yaw moment when the moment required for stability is large. On the other hand, the torque will also decrease when the driving motor operates at a high speed, which is not

conducive to the stability control of an electric vehicle. Although a traditional electronic stability program (ESP) can avoid the issues associated with the disadvantages of the motor, it is not appropriate to directly apply a traditional ESP to an EWV. The traditional ESP uses a hydraulic system as the only actuator of the control system (Zanten et al., 1998; Zanten, 2000). Although the traditional ESP has been widely adopted by the automobile industry, its dynamic performance still has some limitations (Zhang, 2012). There are two main drawbacks: first, the hydraulic ESP system is not sufficiently stable, there is a fluctuation when the hydraulic pressure is under high pressure, and there is still a continuous oscillation after the dynamic process, which makes it difficult to quickly reach a new equilibrium state; the second drawback is that the response is slow, and the response quality is poor. However, if motor driving and hydraulic braking are combined, based on the precise and independent controllable torque characteristics of the four-wheel drive motor of the EWV, precise stability control of the vehicle can be easily realised by assigning different torques to the four driving motors. If the motor cannot achieve the desired yaw moment alone, the hydraulic braking system intervenes and outputs a larger torque in time to fully complement to motor and guarantee the stability of the vehicle.

An electrohydraulic composite stability control system, which integrates the traditional hydraulic braking system and hub motor driving system, is called an electrohydraulic composite ESP in this paper. At present, there are few studies on an electrohydraulic composite ESP for EWVs. The upper controller designed by Zhang (2017) adopts simple PID control based on the yaw rate to achieve an additional yaw torque; therefore, once the parameters are set, the parameters cannot change with different operating conditions, and the influence of the sideslip angle is not taken into account. Therefore, the control effect and precision of this method need to be improved. Ghaffari et al. (2011) proposed a hierarchical control method based on fuzzy theory, which automatically adjusts the wheel slip rate according to the lateral force of the tyres and road adhesion coefficient, thus generating a direct yaw moment. However, fuzzy theory is established based on experience and requires many tests, and it is difficult to calculate the lateral force. The research described by Yang (2013) is relatively comprehensive and has been verified by a simulation and an experiment, but the test effect is general and hydraulic braking is not included. Fu et al. (2018) proposed a novel adaptive sliding mode direct yaw moment control approach to improve the control performance. The proposed strategy enhanced the vehicle's robustness against parametric variations and uncertainties, and this study devised a controller that automatically adapts to changes in the plant parameters, thereby suppressing the effects of estimation errors. However, the strategy still does not take hydraulic braking into account, and most simulation results only present the magnitude of the error for each working condition, not the final control effect of the vehicle.

To overcome the shortcomings of the traditional hydraulic ESP and advance the current research on the electrohydraulic composite ESP, this paper proposes a novel strategy to maintain the manoeuvring stability of EWV by combining the motor system with the hydraulic system. First, models of the hydraulic braking system, electric-driving wheel model, 2-degrees-of-freedom (2-DOF) vehicle reference model and 7-degrees-of-freedom (7-DOF) vehicle model are established. Then, an interacting multiple model state observer (IMM) is established to estimate the sideslip angle in real time. IMM algorithm utilises the weights of linear and nonlinear tyre models based on the unscented Kalman filter (UKF) solves the problem that the sideslip angle is difficult

to measure. Fuzzy sliding mode control (FSMC) is used as the upper level of the hierarchical control structure, and an optimal allocation algorithm is designed for the lower level (Lin, 2015; Osborn and Shim, 2004). Finally, the effectiveness of the system is verified in a joint simulation with CarSim and MATLAB/Simulink, and the validity and rationality of the results are demonstrated.

The paper is organised as follows. Section 2 describes the structural components and working principle of the electrohydraulic ESP system. In Section 3, the establishment and basis of each model used in this paper are described. Section 4 introduces the IMM state observer, upper and lower controllers of the hierarchical control strategy. The principle of fuzzy sliding mode control and an optimal allocation method based on the minimum tyre utilisation ratio are also described. Section 5 presents the joint simulation results of Simulink and CarSim based on the above research and explains the contents of each figure. The content and results of the research are summarised in Section 6, and future work is proposed.

2 Electrohydraulic ESP analysis

2.1 Structural components

An electrohydraulic composite ESP for vehicle control needs to coordinate various sensors and judge the current stability of the automobile body by obtaining information from these sensors (Reif, 2014). Figure 1 shows the main components of the electrohydraulic composite ESP, including the steering wheel angle sensor, yaw rate sensor and lateral acceleration sensor, wheel speed sensor, wheel cylinder pressure sensor, hydraulic control unit, motor control unit and vehicle control unit. The angle sensor is used to identify the steering angle, and the wheel speed sensor, yaw rate sensor and lateral acceleration sensor are used to monitor the motion of the vehicle. The wheel cylinder pressure sensor is used to identify the braking force. The vehicle control unit is used to determine whether the vehicle needs stability control and to transmit the required drive/brake information to the corresponding control unit, which is then distributed to the actuator. The electrohydraulic composite ESP proposed in this paper should be stored in vehicle control unit. In particular, the electrohydraulic composite ESP uses the hydraulic control unit and the wheel hub motor driving system as two sets of independent actuators, which are respectively used to adjust the braking pressure of the controlled wheel and the motor output driving torque to introduce an additional yaw moment to the vehicle and achieve stability control of the vehicle.

2.2 Working principle

In this paper, the stability control system of the electrohydraulic composite ESP is applied to an EWV, which integrates the traditional hydraulic ESP and direct yaw moment control (DYC) (Lan and He, 2015). The basic working principle of the electrohydraulic composite ESP is to determine the current body stability by judging important body characteristics, such as the yaw rate and the centroid sideslip angle, and to modify the instability by a series of control methods, namely, by applying an additional yaw moment to the vehicle body by controlling the differential speed of the wheels. The additional yaw moment can restrain the steering of the vehicle to make the

vehicle have moderate insufficient steering under dangerous conditions, thus maintaining the stability of the vehicle.

Figure 1 Composition of ESP system (see online version for colours)

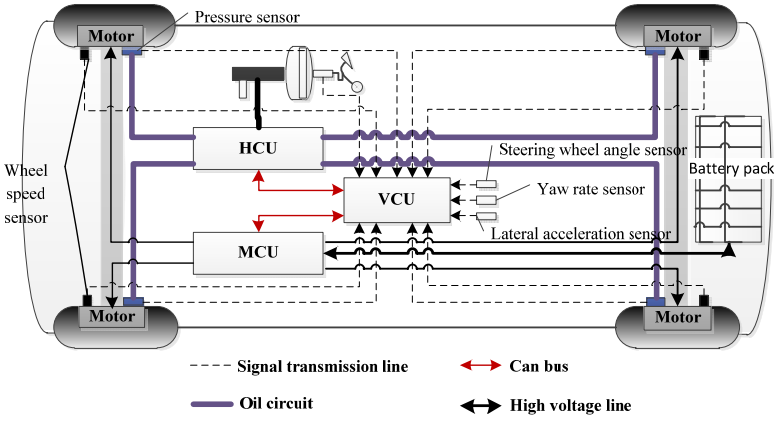

In fact, the sideslip angle is difficult to obtain, so the accurate estimation of the sideslip angle is the first problem to be solved in this paper, which provides the necessary parameters for the design of the following controller. At present, there are many control methods that are used to calculate the additional yaw moment based on body motion parameters. Considering the working condition of the vehicle stability system, this paper selects FSMC method with strong robustness and adaptability to various extreme conditions. The largest difference between the electrohydraulic composite ESP and the traditional hydraulic ESP is that the EWV is equipped with two sets of fully independent and structurally complete actuators, which leads to two heterogeneous variables, the hydraulic braking moment and the motor driving moment, when the control target is allocated to four wheels. Therefore, another focus of this paper is the lower level allocation controller.

3 Establishment of system model

3.1 Establishment of hydraulic braking system model

Considering the complexity of the actual ESP hydraulic system model, the hydraulic model established in this paper focuses on the pressure increase, holding, and decrease processes. The hydraulic system model is established as follows (Peng et al., 2008):

$$\frac{dp_w}{dt} = \begin{cases} 35.7418\left(p_m - p_w\right)^{0.58} & \text{Increasing} \\ 0 & \text{Holding} \\ -36.3714\left(p_w - p_r\right)^{0.92} & \text{Decreasing} \end{cases} \tag{1}$$

There exists a delay in the hydraulic braking system, and the delay in the pressure increase process is greater than the delay in the pressure decrease, which leads to slow action in the initial stage of the stability control. The motor system can be used for control at the beginning of the stability control, because the motor system has a quick response and a short delay, and when the hydraulic system reaches the target value, the motor system gradually stops being implemented for control.

3.2 Electric-driving wheel model

As an important part of electric wheel vehicle, EWV uses four-wheel hub motors instead of traditional internal combustion engine as power output, which makes the motors integrate with tyres. As the main research content of this paper is the method of controlling the direct yaw moment, and the motor control technology is currently relatively mature, this paper does not focus on the performance of motor control but simplifies the electromagnetic conversion process of the motor into a second-order transfer function mathematical model (Duan and Wang, 2015):

$$G(s) = \frac{T_{mi}}{T_{mdi}} = \frac{1}{2\xi^2 s^2 + 2\xi s + 1} \tag{2}$$

where T_{mi} represents the actual torque value of each hub motor, T_{mdi} represents the expected torque value of each hub motor and ζ represents the damping ratio that is related to the parameters of the hub motor.

The accuracy of tyre model largely determines the accuracy of vehicle state parameter estimation. At present, tyre magic formula is most widely used, because it can reflect the tyre state information under different conditions and has strong versatility. However, there are too many parameters in the magic formula model, so it is very difficult to fit and estimate the parameters according to the test data, which makes it difficult to apply to the design of automobile control system (Wang et al., 2000).

In this paper, the method of switching the linear tyre model and the nonlinear tyre model according to the working conditions is adopted when estimating the vehicle state parameters. When the tyre lateral force and sideslip angle are linear, the tyre longitudinal force and lateral force are as follows:

$$\begin{cases} F_y = -C_y \alpha \\ F_x = k_\mu \lambda F_z \end{cases} \tag{3}$$

When the tyre lateral force and sideslip angle are nonlinear, the Dugoff tyre model can be modified as follows:

$$\begin{cases} F_y = \dfrac{C_y \tan\alpha}{1-\lambda} f(s) \\ F_x = \dfrac{C_x \lambda}{1-\lambda} f(s) \end{cases} \tag{4}$$

$$f(s) = \begin{cases} s(2-s) & s < 1 \\ 1 & s \geq 1 \end{cases} \tag{5}$$

$$s = \frac{\mu F_z (1-\lambda_x)}{2\sqrt{C_x^2 \lambda_x^2 + C_y^2 \tan^2 \alpha}} \tag{6}$$

3.3 Electric-driving wheel model

A linear 2-DOF manipulation dynamic model is selected to calculate the expected values because of its simplicity; the model contains several of the most important quantities that are used to reflect the lateral movement of an automobile, such as the body mass, front and rear axle lateral stiffness, and axle distance.

Figure 2 2-DOF vehicle dynamics model (see online version for colours)

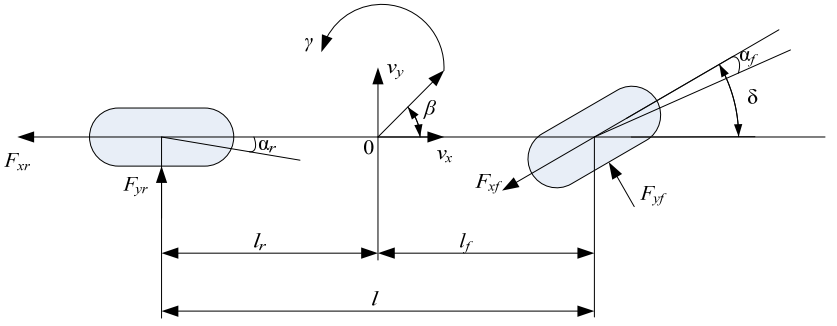

The dynamic equations of the body motion are

$$\left(k_f + k_r\right)\beta + \frac{1}{v_x}\left(l_f k_f - l_r k_r\right)\gamma - k_f \delta = m\left(\dot{v}_y + v_x \gamma\right) \tag{7}$$

$$\left(l_f k_f - l_r k_r\right)\beta + \frac{1}{v_x}\left(l_f^2 k_f + l_r^2 k_r\right)\gamma - l_f k_f \delta = I_z \dot{\gamma} \tag{8}$$

where δ denotes the wheel steering angle; I_Z is the moment of inertia of the vehicle around the z axis; l_f and l_r represent the distances from the centre of mass to the front axle and rear axle, respectively; v_x is the longitudinal velocity of the centre of mass and v_y is the lateral velocity of the centre of mass; γ represents the yaw rate; and k_f and k_r are the cornering stiffnesses of the front wheel and rear wheel, respectively.

The expected yaw rate γ_d and the expected centroid sideslip angle β_d can be calculated as follows:

$$\gamma_d = \frac{v_x}{L\left(1 + K\left|v_x\right|^2\right)}\delta \tag{9}$$

$$\beta_d = \frac{2l_r\left(l_f + l_r\right)k_f k_r - m v_x^2 l_f k_f}{2l_r\left(l_f + l_r\right)^2 k_f k_r - m v_x^2\left(l_f k_f - l_r k_r\right)}\delta \tag{10}$$

where $K = \frac{m}{L^2}\left(\frac{l_f}{k_r} - \frac{l_r}{k_f}\right)$ is a stability factor and an important parameter to characterise the steady-state response of an automobile.

3.4 7-DOF vehicle model

The 7-DOF vehicle model includes the motion equations of the longitudinal, lateral, and yaw directions and the four wheels of the vehicle. Formulas (11)~(13) are the vehicle longitudinal motion equation, lateral motion equation and yaw motion equation, respectively. This model will be used to estimate the sideslip angle in this paper.

$$ma_x = m\left(\dot{v}_x - \omega_r \cdot v_y\right) = \left(F_{xfl} + F_{xfr}\right)\cos\delta - \left(F_{yfl} + F_{yfr}\right)\sin\delta + F_{xrl} + F_{xrr} \tag{11}$$

$$ma_y = m\left(\dot{v}_y + \omega_r \cdot v_x\right) = \left(F_{xfl} + F_{xfr}\right)\sin\delta + \left(F_{yfl} + F_{yfr}\right)\cos\delta + F_{yrl} + F_{yrr} \tag{12}$$

$$\begin{aligned} I_z \cdot \dot{\omega}_r = &\left[\left(F_{xfl} + F_{xfr}\right)\sin\delta + \left(F_{yfl} + F_{yfr}\right)\cos\delta\right] l_f \\ &+ \left[\left(F_{xfr} - F_{xfl}\right)\cos\delta + \left(F_{yfl} - F_{yfr}\right)\sin\delta\right]\frac{t_{w1}}{2} \\ &+ \left(F_{xrr} - F_{xrl}\right)\frac{t_{w2}}{2} - \left(F_{yrl} + F_{yrr}\right) l_r \end{aligned} \tag{13}$$

where δ is the steering angle of the front wheels, and v_x and v_y are the longitudinal vehicle speed and lateral vehicle speed, respectively. F_{xi}, F_{yi} and F_{zi} are the tyre longitudinal force, lateral force and vertical force, respectively, and t_{w1} and t_{w2} are the treads of the front wheels and rear wheels, respectively.

4 Stability control strategy

The structure of the electrohydraulic ESP control strategy is schematically shown in Figure 3. The stability control system of the EWV adopts a hierarchical structure. The control process fully utilises the measurement parameters from the wheel speed sensor, yaw rate sensor, lateral acceleration sensor and front wheel steering angle. Because the sideslip angle is difficult to obtain directly, the IMM-UKF state observer is designed. The design of hierarchical control is carried out after all parameters can be obtained. The control objective of the upper controller is to ensure the yaw stability of the whole vehicle and to provide an ideal yaw moment; the lower controller controls the torque of the four hub motors and the braking hydraulic pressure of the four hydraulic break cylinders independently to ensure that the differential drive of the motor and the differential braking of the hydraulic system can accurately realise the ideal yaw moment and finally coordinate the stability control of the vehicle (Zhang et al., 2012).

Figure 3 Structural chart of stability control strategy (see online version for colours)

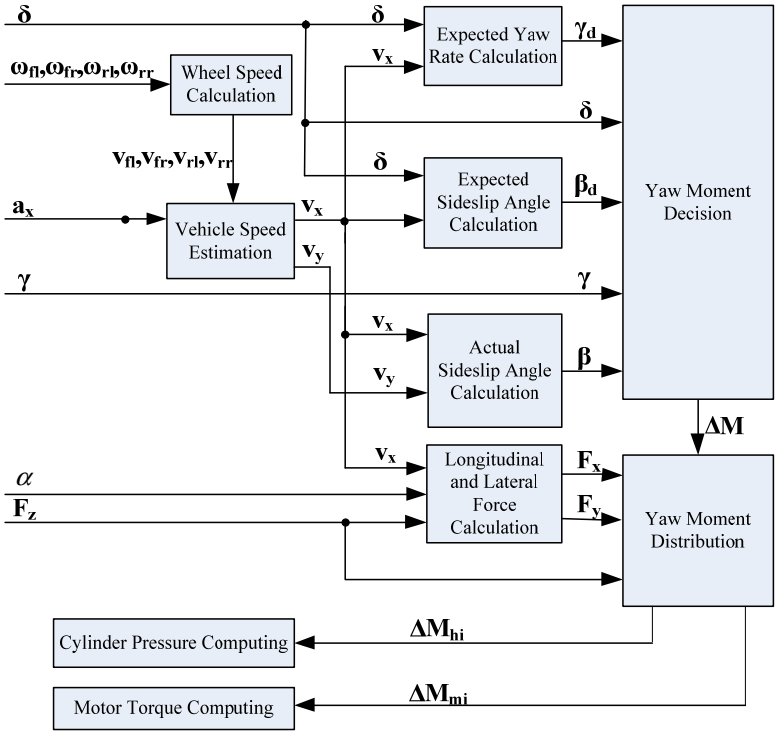

4.1 Upper coordination controller design

4.1.1 IMM-UKF state observer

The ESP system uses the yaw rate and sideslip angle as the control reference quantity. The yaw rate can be measured directly by a sensor, while the sideslip angle cannot be easily measured directly by a sensor. At present, the main method for estimating the sideslip angle is based on Kalman filter optimisation; this paper chooses UKF which has higher control precision than EKF. When the target suddenly changes from the stable state (sudden turn or acceleration), it is difficult to get ideal results by using only a single tyre model. In this paper, a soft hand-over algorithm based on multi-model interaction is used to estimate the real-time parameters of the vehicle according to the different vehicle running state, and UKF is introduced into the IMM algorithm (Baffet et al., 2007). The algorithm structure is shown in Figure 4.

Figure 4 IMM-UKF algorithm structure (see online version for colours)

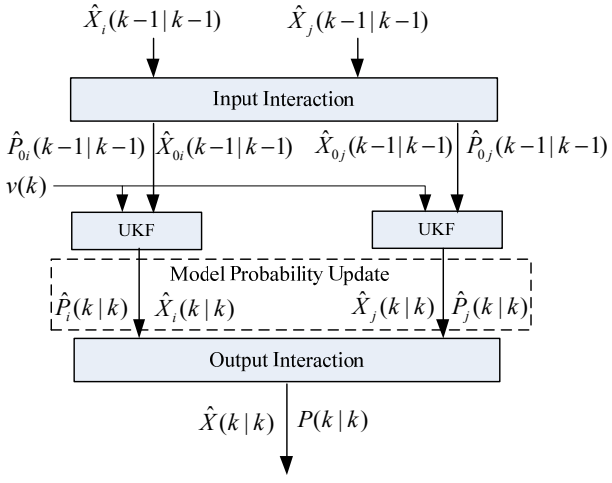

The vehicle model and tyre model have an important role in the accuracy of speed estimation. Therefore, based on the 7DOF vehicle model and tyre model mentioned above, an IMM-UKF state observer is used to estimate the vehicle speed. After that, the sideslip angle can be obtained from the following formula:

$$\beta = \arctan\left(\frac{v_y}{v_x}\right) \tag{14}$$

The state equation and observation equation of the nonlinear system are established according to the previous equation of vehicle motion as follows:

$$\begin{pmatrix} v_x \\ v_y \\ \gamma_r \end{pmatrix}_k = \begin{pmatrix} v_x \\ v_y \\ \gamma_r \end{pmatrix}_{k-1} + \begin{pmatrix} \dot{v}_x \\ \dot{v}_y \\ \dot{\gamma}_r \end{pmatrix} \bullet \Delta t + w(t) \tag{15}$$

$$\begin{pmatrix} a_x \\ a_y \\ \gamma_r \end{pmatrix}_k = \begin{pmatrix} \left[\left(F_{xfl} + F_{xfr}\right)\cos\delta - \left(F_{yfl} + F_{yfr}\right)\sin\delta + F_{xrl} + F_{xrr}\right]/m \\ \left[\left(F_{xfl} + F_{xfr}\right)\sin\delta + \left(F_{yfl} + F_{yfr}\right)\cos\delta + F_{yrl} + F_{yrr}\right]/m \\ \gamma_r \end{pmatrix}_k + v(t) \tag{16}$$

Choose the state vector $x = (v_y\ v_x\ \gamma_r)^T$, the measurement vector $y = (a_y\ a_x\ \gamma_r)^T$, and the input variable $u = (\delta\ T_{ij}\ \gamma_{ij})$. $w(t)$ and $v(t)$ are the process noise and the observation noise, respectively; assuming they are independent white Gaussian noise, the mean values are q_k and r_k, respectively, and the covariances are Q_k and R_k respectively. Longitudinal force F_x and lateral force F_y are calculated by tyre model. The transfer between linear and nonlinear tyre models is determined by Markov probability transfer matrix. The IMM algorithm is carried out in a recursive manner. It is mainly divided into the following steps:

Step 1 Input interaction: the linear tyre model is modelled as model *i*, the nonlinear tyre model is modelled as model *j*, and P_{ij} represents the probability of transferring from the linear tyre model to the nonlinear tyre model. The prediction probability of model *j* is as follows:

$$\overline{c}_j = \sum_{i=1}^{r} P_{ij}\mu_j(k-1) \tag{17}$$

The mixed probability of model *i* to model *j* is:

$$\mu_{ij}(k-1|k-1) = \sum_{i=1}^{r} P_{ij}\mu_i(k-1)/\overline{c}_j \tag{18}$$

Mixed state estimation of model *j*:

$$\hat{X}_{0j}(k-1|k-1) = \sum_{i=1}^{r} \hat{X}_i(k-1|k-1)\mu_{ij}(k-1|k-1) \tag{19}$$

Mixed covariance estimation of model *j*:

$$\begin{aligned} P_{0j}(k-1\,|\,k-1) = \sum_{i=1}^{r} \mu_{ij}(k-1|k-1)\{&P_i(k-1|k-1) \\ &+\left[\hat{X}_i(k-1|k-1) - \hat{X}_{0j}(k-1\,|\,k-1)\right] \\ &\bullet\left[\hat{X}_i(k-1|k-1) - \hat{X}_{0j}(k-1|-1)\right]^T\} \end{aligned} \tag{20}$$

where $\mu_j(k-1)$ is the probability of model *j* at time $k-1$. Mixed state estimation $\hat{X}_{0j}$ and covariance P_{0j} are the initial state of the current cycle.

Step 2 UKF algorithm: after the initial value of time *k* is obtained, UKF is used to update the state of the two models, then the state estimation and error covariance matrix of the two models are obtained. The yaw rate sensor can obtain the yaw rate γ_d in equation of state [equation (15)]. Longitudinal force F_x and lateral force F_y in observation equation [equation (16)] are calculated by linear tyre model and nonlinear tyre model. The other variables can be obtained by sensors. The specific calculation process of UKF algorithm is not discussed in this paper.

Step 3 Model probability update: the likelihood function is used to update the model probability $\mu_j(k)$. The likelihood function of model *j* is:

$$\Lambda_j(k) = \frac{1}{(2\pi)^{n/2}\left|S_j(k)\right|^{1/2}} \exp\left\{-\frac{1}{2} v_j^T S_j^{-1}(k) v_j\right\} \tag{21}$$

where $v_j(k) = Z(k) - H(k)\hat{X}_j(k\,|\,k-1)$, $S_j(k) = H(k)P_j(k\,|\,k-1)H(k)^T + R(k)$.

At present, the probability of model *j* is updated to:

$$\mu_j(k) = \Lambda_j(k)\overline{c}_j/c \tag{22}$$

The normalised constant $c=\sum_{j=1}^{r}\Lambda_j(k)\overline{c}_j$.

Step 4 Output interaction: based on the model probability, the estimated results of each filter are weighted and merged to obtain the total state estimation.

$$\hat{X}(k|k)=\sum_{j=1}^{r}\hat{X}_j(k|k)\mu_j(k) \tag{23}$$

Total covariance estimation:

$$\begin{aligned}P(k|k)=&\sum_{j=1}^{r}\mu_j(k)\{P_j(k\mid k)\\&+\left[\hat{X}_j(k\mid k)-\hat{X}(k\mid k)\right]\bullet\left[\hat{X}_j(k\mid k)-\hat{X}(k\mid k)\right]^T\}\end{aligned} \tag{24}$$

In summary, the total output of the state observer is the weighted average of the estimated results of multiple filters. The weight is the probability that model correctly describes the target motion, which is called model probability.

4.1.2 Additional yaw moment decision module

SMC is characterised by a control discontinuity, and consequently the controlled system is independent of parameter changes and external disturbances and has excellent robustness. One of the keys to realising SMC is the design of the sliding mode surface. The selection of the sliding mode surface should not only satisfy the requirements for tracking the yaw rate but also take into account the tracking of the sideslip angle. It can be seen from the linear 2-DOF vehicle model that there is coupling between β and γ. The sideslip angle can become too large when only the yaw rate is considered, and the vehicle cannot follow the desired yaw rate well when only the sideslip angle is controlled. In brief, controlling β and γ co-ordinately can solve the problems described above. Therefore, define the sliding mode surface as follows:

$$s=\varepsilon\left(\gamma-\gamma_d\right)+\xi\left(\beta-\beta_d\right) \tag{25}$$

The sliding mode surface defines a weighted combination of the yaw rate and the lateral deflection error and takes into account the values of the target's yaw rate in equation (9) and the target lateral deflection angle in equation (10) discussed earlier in this paper.

After differentiating equation (16), the equation can be written as

$$s=\varepsilon\left(\dot{\gamma}-\dot{\gamma}_d\right)+\xi\left(\dot{\beta}+\dot{\beta}_d\right) \tag{26}$$

According to the motion equation of the whole vehicle, $\dot{\gamma}$ in equation (17) can be replaced, and the sliding mode surface is redefined as follows:

$$\dot{s}=\varepsilon\left[-\frac{\left(l_fK_f-l_rK_r\right)}{I}\beta-\frac{\left(l_f^2K_f+l_r^2K_r\right)}{IV}r+\frac{l_fK_f}{I}\delta-\frac{\Delta M}{I}-\dot{r}_d\right]+\xi\left(\dot{\beta}-\dot{\beta}_d\right) \tag{27}$$

In this paper, the exponential approach law is adopted and assumed as follows:

$$\dot{s} = -k \operatorname{sgn} s - bs \tag{28}$$

where $a > 0$, $b > 0$.

The additional yaw moment can be obtained as follows:

$$\begin{aligned} \Delta M = &-\frac{I}{\varepsilon}(-k \operatorname{sgn} s - bs) - \left(l_f K_f - l_r K_r\right)\beta - \frac{\left(l_f^2 K_f + l_r^2 K_r\right)}{V} r \\ &+ l_f K_f \delta - I\dot{r}_d + \frac{I\xi}{\varepsilon}\left(\dot{\beta} - \dot{\beta}_d\right) \end{aligned} \tag{29}$$

4.1.3 Fuzzy sliding mode controller design

According to formula (20), it can be seen that although the existence of symbolic function can eliminate interference terms, it inevitably leads to chattering, and it cannot be changed once the value of switching gain coefficient k is determined, which has certain limitations. In this paper, the traditional SMC is improved by designing fuzzy control, and the switching gain is adjusted appropriately according to the relative position between the system and the sliding surface.

Figure 5 (a) Membership function of switching gain coefficient $k(t)$ (b) Membership function of the product of sliding mode surface function s and its derivative $\dot{s}$ (see online version for colours)

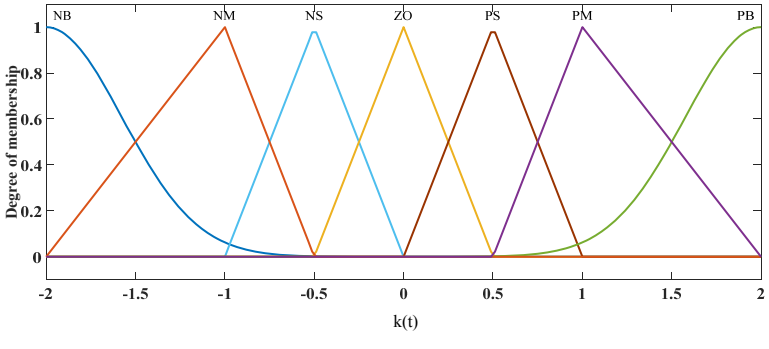

(a)

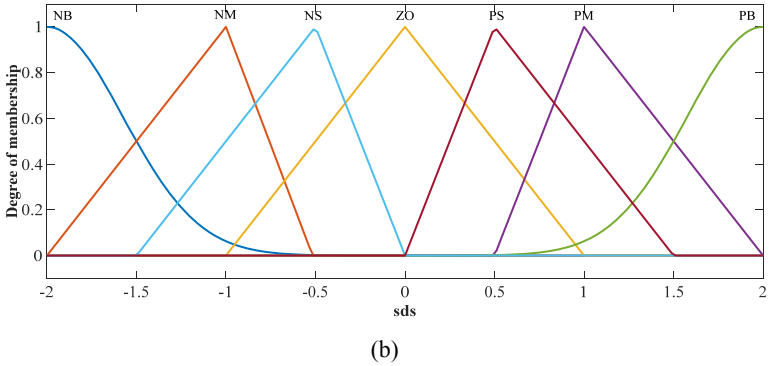

(b)

$s\dot{s}$ is regarded as the fuzzy input, k is regarded as the output, the parameters $s\dot{s}$ and k are transformed into the fuzzy sets of $S[-2, 2]$ and $k[-2, 2]$, respectively, and the corresponding fuzzy linguistic variables are $s\dot{s}$ = {NB NM NS ZO PS PM PB}, and Δk = {NB NM NS ZO PS PM PB}. $s\dot{s} > 0$ indicates that the current state of the sliding mode function is the same as the change trend, and the sliding mode surface tends to be far from the sliding mode surface. The switching gain k should be increased. $s\dot{s} < 0$ indicates that the state of the sliding mode function is opposite of the changing trend at this time, the system is approaching the sliding mode surface, and the switching gain k should be reduced. However, the size of $|s\dot{s}|$ also needs to be considered to further rationalise the design of the fuzzy rules. When $|s\dot{s}|$ is large, $|k|$ should also undergo a larger change, and vice versa. Based on this analysis, the membership function diagram of the fuzzy rules and the fuzzy system can be obtained.

In the design of the fuzzy controller, the design of the fuzzy rules is an important link for determining its performance. In this paper, seven fuzzy rules for the switching gain coefficient $k(t)$ are detailed as follows:

R1 IF $s\dot{s}$ is PB THEN Δk is PB

R2 IF $s\dot{s}$ is PM THEN Δk is PM

R3 IF $s\dot{s}$ is PS THEN Δk is PS

R4 IF $s\dot{s}$ is ZO THEN Δk is ZO

R5 IF $s\dot{s}$ is NS THEN Δk is NS

R6 IF $s\dot{s}$ is NM THEN Δk is NM

R7 IF $s\dot{s}$ is NB THEN Δk is NB.

Finally, the control structure of FSMC as shown in Figure 6 is obtained and the additional yaw moment is calculated.

Figure 6 Control block diagram of FSMC

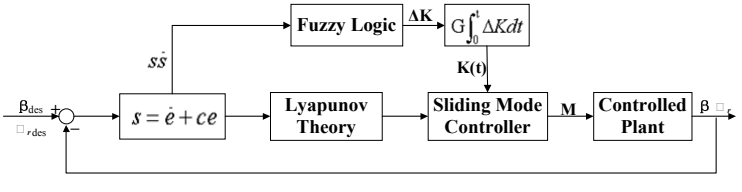

4.2 Lower distribution controller design

Torque distribution control is achieved by the lower level of the vehicle stability control scheme. The function of torque distribution control is to coordinate the control of multiple actuators and convert the generalised force into the output torque for each actuator (He et al., 2006). The advantage of an EWV is that each wheel is independent and controllable and has a fast response. The peak power of the hub motor at a high speed is limited and often cannot meet the torque requirements for stability control under extreme conditions. In this paper, a torque distribution controller is designed considering the advantage that a hydraulic system can provide a larger longitudinal braking force.

An output torque diagram of the actuator during driving conditions is shown in Figure 7 (Li et al., 2017).

Figure 7 Actuator output torque diagram (see online version for colours)

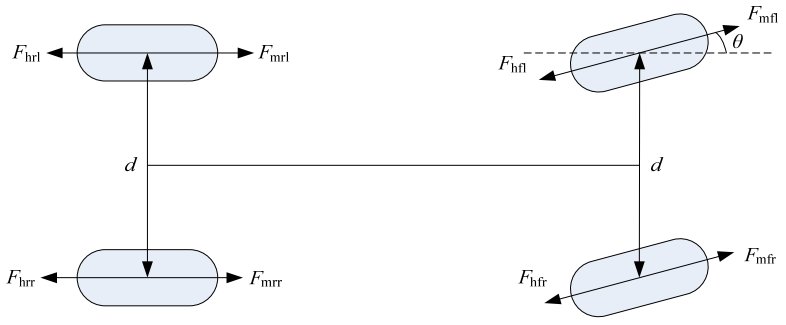

where d stands for the wheelbase, F_{mfl}, F_{mfr}, F_{mrl} and F_{mrr} are the longitudinal force outputs of the left front wheel, right front wheel, left rear wheel and right rear wheel driving motors, and F_{hfl}, F_{hfr}, F_{hrl} and F_{hrr} are the braking force outputs of the left front wheel, right front wheel, left rear wheel and right rear wheel hydraulic braking systems, respectively.

The total longitudinal force and yaw moment of the vehicle are as follows:

$$\begin{cases} F = F_{mfl}\cos\theta + F_{mfr}\cos\theta + F_{mrl} + F_{mrr} - F_{hfl}\cos\theta - F_{hfr}\cos\theta - F_{hrl} - F_{hrr} \\ M_z = \dfrac{d}{2}\left(-F_{mfl}\cos\theta + F_{mfr}\cos\theta - F_{mrl} + F_{mrr} + F_{hfl}\cos\theta - F_{hfr}\cos\theta \right. \\ \qquad \left. + F_{hrl} - F_{hrr}\right) \end{cases} \tag{30}$$

When the current wheel rotation angle is small, $\cos\theta$ is approximately equal to 1.

4.2.1 Optimisation objectives and constraint conditions

At present, the main schemes used for the active brake wheels in the hydraulic system are single-wheel braking and double-wheel braking. While the lower-level distributor of the electrohydraulic composite ESP needs to distribute two target variables (the total longitudinal force and the additional yaw moment) to eight control variables (the four hydraulic braking forces and the four motor driving forces) of two sets of actuators, there is a problem of redundancy in the distribution, so the above two methods are not applicable. Therefore, an optimal allocation algorithm based on the minimum tyre utilisation rate is proposed for the lower-level control of the electrohydraulic composite ESP.

To reasonably distribute the external forces of the EWV, the minimum squared sum of the utilisation ratio of the vehicle for all tyres is regarded as the objective function to distribute the tyre forces (Masato, 2016; Zou et al., 2009). The advantage of this method is that the generalised resultant force of the vehicle can be allocated based on the corresponding optimised longitudinal force and lateral force on the four wheels according to the actual motion state of the vehicle, ensuring that the vehicle can maintain stability and have a greater stability margin under different working conditions. To ensure the

stability of the vehicle, an optimisation objective is introduced to characterise the overall road load state of the vehicle.

$$\min J = \sum_{i=1}^{4} \frac{F_{xi}^2 + F_{yi}^2}{\left(\mu \cdot F_{zi}\right)^2}, \qquad i = fl, fr, rl, rr \tag{31}$$

where μ is the road adhesion coefficient and is assumed to be known; F_{xi} is the longitudinal force of each wheel, F_{yi} is the lateral force of each wheel, and F_{zi} is the vertical load of each wheel.

The magnitude of the torque provided by the motor constrained by the external characteristics of the motor is as follows:

$$-\frac{T_{i\max}(v)}{r} \le F_{mi} \le \frac{T_{i\max}(v)}{r}, \qquad i = fl, fr, rl, rr \tag{32}$$

where $T_{i\max}(v)$ is the peak torque of the motor.

The longitudinal force constrained by the road adhesion conditions and vertical loads can be described as follows:

$$-\mu F_{zi} \le F_{xi} \le \mu F_{zi}, \qquad i = fl, fr, rl, rr \tag{33}$$

4.2.2 Quadratic programming optimisation allocation algorithm

According to the optimisation objectives and constraints above, the standard form of the quadratic programming method is summarised as:

$$\min_{u_c} J = u_c^T W u_c \tag{34}$$

$$\text{Constrained:} \begin{cases} B u_c = u_c^T W u_c \\ u_{c\min} \le u_c \le u_{c\max} \end{cases} \tag{35}$$

where

$$W = diag\left(\frac{1}{\left(\mu F_{zi}\right)^2}\right), \qquad i = fl, fr, rl, rr, fl, fr, rl, rr$$

$$u_c = \begin{bmatrix} F_{mfl} & F_{mfr} & F_{mrl} & F_{mrr} & F_{hfl} & F_{hfr} & F_{hrl} & F_{hrr} \end{bmatrix}^T.$$

The quadprog function in MATLAB can be used to solve the standard quadratic programming problem shown above.

5 Simulation and analysis

5.1 Verification of estimation effect of state observer

It is necessary to compare the deviation between the actual centroid sideslip angle and the value estimated earlier in this paper. Simulation results for the steering wheel angle step

input test at an initial vehicle speed of 80 km/h and road adhesion coefficient is set to 0.3 are shown in Figures 8 and 9.

Figure 8 Standard deviation of estimation errors for longitudinal and lateral speed (see online version for colours)

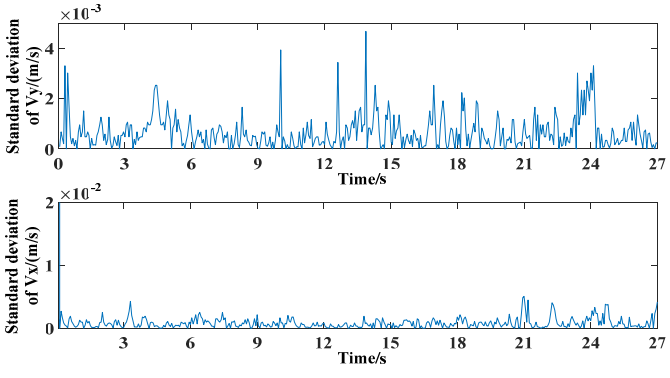

Figure 9 Comparisons of the moving paths of the centre of mass (see online version for colours)

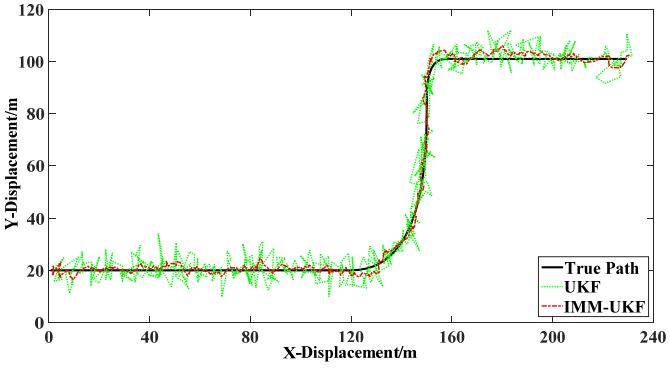

Because the accuracy of the sideslip angle comes from v_x and v_y, the estimation errors of v_x and v_y fundamentally determine the estimation errors of the sideslip angle, and the standard deviation of the estimation error of v_x and v_y is shown in Figure 8. Although v_x has a large standard deviation at the beginning, it decreases rapidly and keeps the standard deviation within 0.01 m/s. The standard deviation of the estimated value v_y is always within 0.005 m/s, which also has high estimation accuracy. In order to show the estimation accuracy of v_y and v_x more simply and intuitively, this paper calculates the path corresponding to the velocity estimation by integrating the velocity at each moment, and compares it with UKF calculated by nonlinear tyre model. Figure 9 shows that IMM-UKF algorithm is closer to the real path, proving that the v_x and v_y estimated in this paper close to the actual value, so the subsequent simulation is effective and agrees with the actual situation.

5.2 Establishment of CarSim vehicle simulation model

To verify the effectiveness of the proposed electrohydraulic composite control strategy, a simulation is carried out in CarSim. CarSim is specialised dynamic simulation software that provides a multifarious test environment and supplies ports to Simulink for reading and writing data. CarSim is utilised to build a complete vehicle model of an EWV for different emulation working conditions. MATLAB/Simulink is used to build the desired control strategy. Since CarSim software does not have a simulation module for an EWV, this paper uses CarSim to build the whole vehicle model according to the characteristics of the EWV. The parameters of the electric vehicle are shown in Table 1.

Table 1 Vehicle parameters

Parameters	*Unit*	*Value*
Mass	kg	1,240
Wheelbase	mm	2,610
Distance from centre of mass to front axle	mm	1,157
Distance from centre of mass to rear axle	mm	1,453
Yaw moment of inertia	$kg \cdot m^2$	1,662
Front tread	mm	1,464
Rear tread	mm	1,464
Height of centre of mass	mm	510
Wheel rolling radius	mm	307

An EWV is an electric vehicle driven by the hub motor placed in the rim, so the hub motor and tyre are regarded as a whole and a non-spring-loaded mass. Therefore, the non-spring-loaded mass of a single tyre of the EWV is 40 kg, and the moment of inertia of the non-spring-loaded mass can be calculated as follows:

$$J_z = m_f r^2 \tag{36}$$

where m_f is the non-spring-loaded mass and r is the static load radius (the value of r can be replaced by the wheel rolling radius).

The power of the EWV is supplied by the permanent magnet brushless DC motor installed in the wheels, so it is necessary to improve the vehicle model in CarSim and change the transmission system in CarSim to four-wheel-drive mode (Ma and Li, 2015). This is achieved by interrupting the power transmission, considering the components of the vehicle transmission system in the spring load quality and then changing the transmission system in CarSim to four-wheel-drive mode. The output torque of the motor is loaded directly to the wheels, which is based on the CarSim simulation model of the electric wheel motor drive system, as shown in Figure 10. In Figure 10, IMP_MVBK represents the hydraulic braking torque, and IMP_MY_OUT represents the driving torque output of the motor.

Figure 10 CarSim electric vehicle model power system and input settings (see online version for colours)

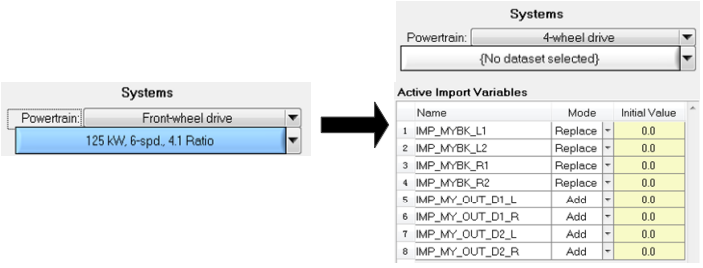

As the research objective of this paper is based on an EWV, the simulation adopts the composite ESP, DYC with the motor only and no control in three cases for a comparison. To profoundly reflect the advantages of the composite ESP, two conditions are simulated:

1 a double shift line on a low-adhesion road surface ($\mu = 0.5$)

2 continuous sinusoidal input on a low-adhesion road surface ($\mu = 0.2$).

5.3 Simulation of double shift line on low adhesion road surface

Figures 11–14 show the simulation results of a vehicle at a speed of 50 km/h under double lane change conditions with a road adhesion coefficient of 0.5.

Figure 11 Steering wheel angle input (see online version for colours)

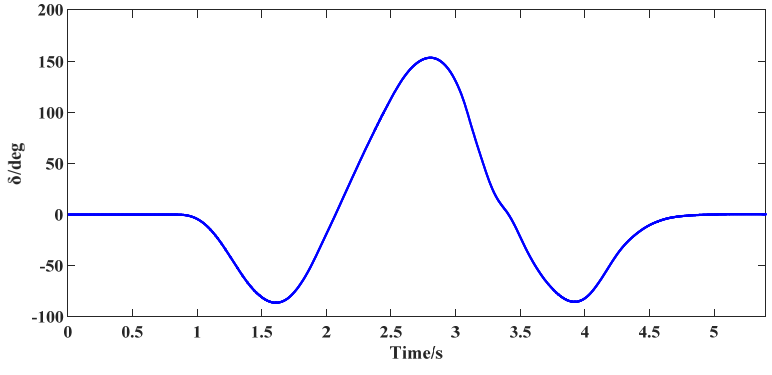

In this simulation, the results of the electrohydraulic composite ESP, direct yaw control (DYC) with the motor only and no control are compared under this working condition. The results are as follows: Figure 11 shows the input characteristics of the steering wheel under this condition. The results will prove that the control is effective if the vehicle path can reflect the input well. Figure 12(a) shows the response curve of the vehicle yaw rate. The steering wheel angle input is larger between 3 and 3.5 s. At this time, the electrohydraulic composite ESP can provide a larger additional yaw moment to quickly restore the vehicle stability. At this stage, the yaw rate can be reduced by an average of 6.7894 deg/s with the composite ESP in 0.1 s, which is 14.3% higher than that achieved with DYC. Moreover, it is obvious that the uncontrolled vehicle has completely lost its stability. Figure 12(b) shows that the centroid sideslip angle of the vehicle controlled by

DYC fluctuates greatly during the second lane change, resulting in vehicle instability. However, the coordinated control of the electrohydraulic composite ESP can keep the centroid sideslip angle within a very small range (±1 deg) and maintain the vehicle stability. In addition, as can be seen from the figure, the electrohydraulic composite ESP ensures that the vehicle can better follow the driving intentions (steering wheel input) than the other two cases. To obtain a more intuitive understanding of the control effect, Figure 12(c) shows the path of the vehicle. It is clear that the uncontrolled vehicle path deviates greatly from the desired path; the electrohydraulic composite ESP restores the stability at 55 metres, while DYC completely loses stability after 55 metres and cannot quickly restore the stable state.

Figure 12 (a) Vehicle yaw rate response (b) Vehicle centroid sideslip angle (c) Vehicle path diagram (see online version for colours)

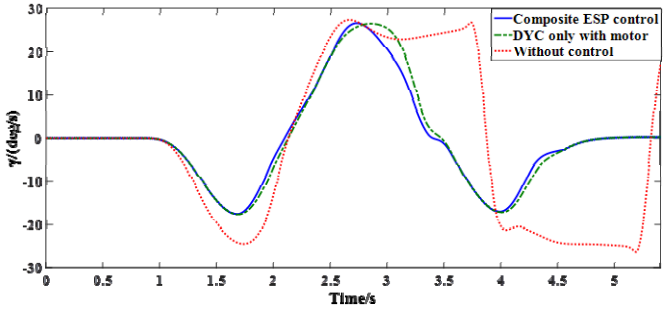

(a)

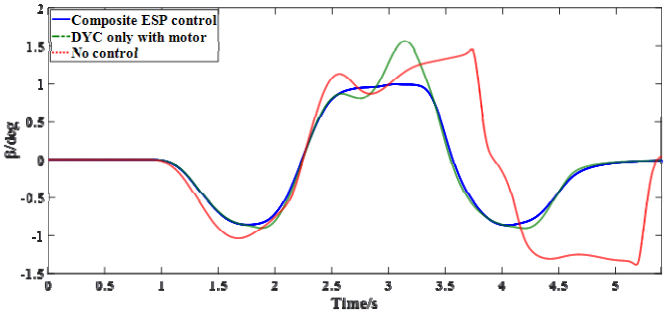

(b)

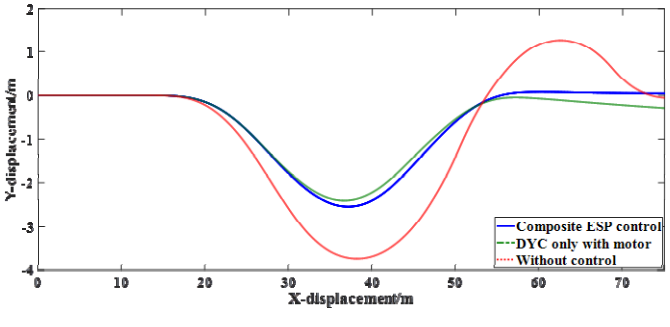

(c)

5.4 Simulation of continuous sinusoidal input on low adhesion road surface

The continuous sinusoidal input condition for the steering wheel angle is also a classic stability test condition. Usually, we use this condition to simulate a single lane change of a vehicle. Therefore, to make the results more convincing, this paper also verifies the effect of the coordinated control of the electrohydraulic composite ESP under this condition. The specific working conditions are as follows: the road adhesion coefficient is 0.2, the vehicle speed is 100 km/h, the sinusoidal input of the steering wheel angle is as shown in Figure 13, the amplitude of the sinusoidal signal is 90 deg and the period is 6 s.

Figure 13 Steering wheel angle input (see online version for colours)

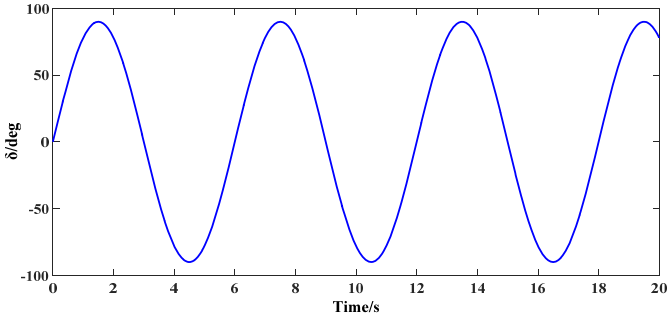

Figure 14 (a) Vehicle yaw rate response (b) Vehicle centroid sideslip angle (c) Vehicle path diagram (see online version for colours)

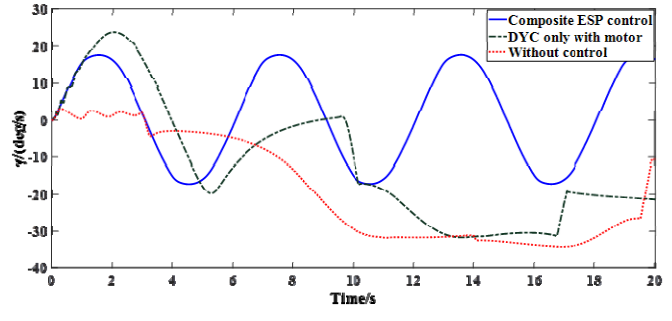

(a)

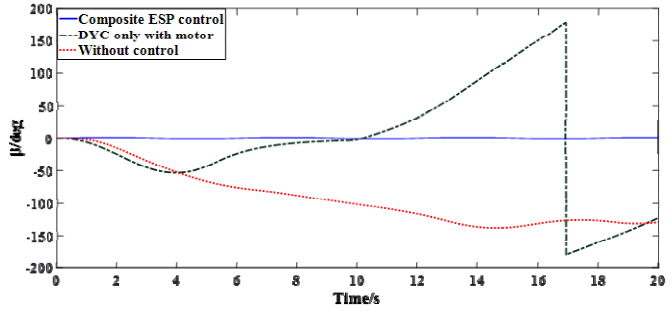

(b)

Figure 14 (a) Vehicle yaw rate response (b) Vehicle centroid sideslip angle (c) Vehicle path diagram (continued) (see online version for colours)

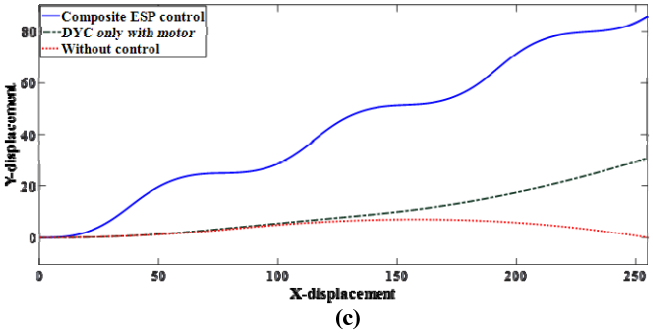

(c)

The response curve of the vehicle yaw rate is shown in Figure 14(a). It can be clearly seen that the vehicle with DYC or without control is basically out of control during the second steering occurrence (at approximately 5 s), while the vehicle with the composite ESP can maintain the yaw rate within a stable region (±20 deg/s) and the response basically corresponds to the input. Figure 14(b) clearly shows that the control system of the composite ESP proposed in this paper almost maintains the centroid sideslip angle near 0 deg, which greatly improves the stability of the vehicle and avoids drift and sideslip. In Figure 14(c), we can see the difference between the three actual paths of the vehicle. EWV with the composite ESP have a better ability to drive according to the driver's control intentions, and there is no sideslip or other instability. Conversely, the uncontrolled vehicles and DYC-equipped vehicles lose control almost at the first turn, and the stability cannot be restored.

6 Conclusions and recommendations

Most of the existing control methods for the stability of an EWV use a motor as a single actuator, which may not be able to provide a sufficient yaw moment to maintain stability under certain limiting conditions. To guarantee the handling stability of an EWV, this paper proposes an electrohydraulic composite electronic stability program based on hierarchical control. The yaw moment that is employed to ensure vehicle stability is calculated by the upper FSMC controller, and the lower distribution controller determines the distribution of additional yaw moment based on the quadratic programming method. A hydraulic system, a 2-DOF vehicle model, an electric-driving wheel model and a 7-DOF vehicle model are also established. Then, IMM-UKF algorithm is employed to estimate vehicle speed and sideslip angle. Finally, a joint simulation of the whole control structure and models is carried out in CarSim and Simulink. Finally, the results of the conventional DYC control scheme, the case without control and the composite ESP method are compared under different conditions. The conclusions are presented as follows:

1 The simulation results show that the estimation methods and models used in this paper are in line with the actual situation and have desired control effect, which make the simulation results convincing.

2 Comparing the electrohydraulic composite control strategy and DYC with the motor only, the former shows a more stable response and restores the stability faster in two conditions, especially under extreme conditions. Moreover, the vehicle path of the former is closer to the driver's expected response.

3 Compared with the simulation under the two conditions, it is clearly found that the control effect of the electrohydraulic composite ESP proposed in this paper is more obvious for the extreme conditions of low adhesion and frequent steering. This result is consistent with the purpose of this study; therefore, the research objectives have been achieved.

The proposed electrohydraulic composite control system can guarantee that the vehicle maintains the expected path even under extreme working conditions and can control the yaw rate and centroid sideslip angle within ideal ranges. Future research will focus on improving the response speed and control accuracy of the system under as many conditions as possible to further improve the safety and reliability of electric wheeled vehicles.

Acknowledgements

The authors disclosed receipt of the following financial support for the research, authorship, and publication of this article: this work was supported by the national key research and development plan program under grant 2018YFB0104803, the Six Talent Peaks Project of Jiangsu Province under grant JXQC-042; the Primary Research and Development Plan of Jiangsu Province under grant BE2017129; and Key Laboratory of Road and Traffic Engineering of the Ministry of Education, Tongji University under grant K201903.

References

Baffet, G., Charara, A. and Lechner, D. (2007) 'Estimation process for tire-road forces and vehicle side-slip angle', *4th International Conference on Informatics in Control, Automation and Robotics*, pp.5–10, INSTICC Press, Angers.

Duan, T. and Wang, C. (2015) 'Sliding mode-PID control of driving system for motorized wheels vehicle', *Journal of Jiangsu University (Natural Science Edition)*, Vol. 36, No. 3, pp.261–264.

Fu, C., Hu, M. et al. (2018) 'A novel adaptive sliding mode control approach for electric vehicle direct yaw-moment control', *Advances in Mechanical Engineering*, Vol. 10, No. 10, pp.1–12.

Ghaffari, A., Oreh, S.H.T., Kazemi, R. et al. (2011) 'An intelligent approach to the lateral forces usage in controlling the vehicle yaw rate', *Asian Journal of Control*, Vol. 13, No. 2, pp.213–231.

He, J., Crolla, D.A., Levesley, M.C. and Manning, W.J. (2006) 'Coordination of active steering, driveline, and braking for integrated vehicle dynamics control', *Proceedings of the Institution of Mechanical Engineers Part D*, 220(D10), pp.1401–1420.

Jin, X., Yin, G., Li, Y. and Li, J. (2015) 'Stabilizing vehicle lateral dynamics with considerations of state delay of AFS for electric vehicles via robust gain-scheduling control', *Asian Journal of Control*, Vol. 18, No. 1, pp.89–97, doi: 10.1002/asjc.1161.

Lan, F. and He, X. (2015) 'Investigation into handling and stability of 4WD electric vehicle based on electro-hydraulic control', *Journal of South China University of Technology (Natural Science Edition)*, Vol. 43, No. 8, pp.62–68.

Li, B., Du, H., Li, W. and Zhang, B. (2017) 'Integrated dynamics control and energy efficiency optimization for overactuated electric vehicles', *Asian Journal of Control*, doi: 10.1002/asjc.1686.

Lin, C. (2015) 'Stability hierarchical control strategy for distributed-driving electric vehicle', *Transactions of Beijing*, Vol. 35, No. 5, pp.490–493.

Ma, G. and Li, G. (2015) 'Simulation model research for four-wheel hub motor electric vehicle based on Simulink and CarSim', *Agricultural Equipment & Vehicle Engineering*, Vol. 53, No. 7, pp.8–11.

Masato, A. (2016) *Vehicle Handling Dynamics – Theory and Application*, 2nd ed., pp.212–216, China Machine Press, China.

Murata, S. (2010) 'Innovation by in-wheel-motor drive unit', *10th International Symposium on Advanced Vehicle Control*, 22–26 August.

Osborn, R.P. and Shim, T. (2004) *Independent Control of All-Wheel-Drive Torque Distribution*, SAE Technical Paper Series, 01-2052.

Peng, D., Zhang, Y., Yin, C-L. and Zhang, J-W. (2008) 'Combined control of a regenerative braking and anti-lock braking system for hybrid electric vehicles', *International Journal of Automotive Technology*, Vol. 9, No. 5, pp.749–757.

Reif, K. (2014) *Brakes, Brake Control and Driver Assistance Systems*, Springer, Friedrichshafen.

Wang, D., Guo, K. and Zong, C. (2000) 'Theoretical study on vehicle dynamic stability control', *Automotive Engineering*, Vol. 22, No. 1, pp.8–12.

Yang, P. (2013) 'Stability control strategy design and experiment of distributed electric drive vehicle', *Journal of Mechanical Engineering*, Vol. 49, No. 24, pp.128–143.

Zanten, A.T.V. (2000) 'Bosch ESP systems: 5 years of experience', *SAE 2000 Automotive Dynamics & Stability Conference*.

Zanten, A.T.V., Erhardt, R., Landesfeind, K. et al. (1998) 'VDC systems development and perspective', *Vacuum*, Vol. 28, No. 12, p.429.

Zhang, H. (2012) *Analyse and Control of Electro Hydraulic Braking System for Vehicle*, Nanjing University of Aeronautics and Astronautics, Nanjing.

Zhang, H. (2017) 'Research on coordinated control of electro-hydraulic compound ESP for electric wheel', *Journal of Guangxi University (Nat. Sci. Ed.)*, Vol. 42, No. 2, pp.442–451.

Zhang, J-Z., ZHANG, H-T. and SUN, Y-T. (2012) 'The direct yaw control of electric vehicle stability control', *Electric Machines and Control*, Vol. 16, No. 6, pp.75–80.

Zhu, W., Luo, Y., Han, Y. et al. (2012) 'Rule-based traction system failure control of distributed electric drive vehicle', *Journal of Mechanical Engineering*, Vol. 48, No. 10, pp.90–96.

Zou, G., Luo, Y. and Li, K. (2009) 'Tire longitudinal force optimization distribution for independent 4WD EV', *Journal of Tsinghua University (Science and Technology)*, Vol. 49, No. 5, pp.721–727.

Abbreviations

EWV	Electric wheeled vehicle.
ESP	Electronic stability program.
IMM-UKF	Interacting multiple model-unscented Kalman filter.
FSMC	Fuzzy sliding mode control.